

Coordinated Trajectories for Non-stop Flying Carriers Holding a Cable-Suspended Load

Chiara Gabellieri¹ and Antonio Franchi²

Transportation Research Record
2025, Vol. XX(X) 1–11
©National Academy of Sciences:
Transportation Research Board 2025
Article reuse guidelines:
sagepub.com/journals-permissions
DOI: 10.1177/ToBeAssigned
journals.sagepub.com/home/trr

SAGE

Abstract

Multirotor UAVs have been typically considered for aerial manipulation, but their scarce endurance prevents long-lasting manipulation tasks. This work demonstrates that the non-stop flights of three or more carriers are compatible with holding a constant pose of a cable-suspended load, thus potentially enabling aerial manipulation with energy-efficient non-stop carriers. It also presents an algorithm for generating the coordinated non-stop trajectories. The proposed method builds upon two pillars: (1) the choice of n special linearly independent directions of internal forces within the $3n - 6$ -dimensional nullspace of the grasp matrix of the load, chosen as the edges of a Hamiltonian cycle on the graph that connects the cable attachment points on the load. Adjacent pairs of directions are used to generate n forces evolving on distinct 2D affine subspaces, despite the attachment points being generically in 3D; (2) the construction of elliptical trajectories within these subspaces by mapping, through appropriate graph coloring, each edge of the Hamiltonian cycle to a periodic coordinate while ensuring that no adjacent coordinates exhibit simultaneous zero derivatives. Combined with conditions for load statics and attachment point positions, these choices ensure that each of the n force trajectories projects onto the corresponding cable constraint sphere with non-zero tangential velocity, enabling perpetual motion of the carriers while the load is still. The theoretical findings are validated through simulations.

Introduction

Aerial manipulation has been intensely studied thanks also to the potential impact in many different real-world use cases. Interesting applications are, e.g., parcel delivery and assembly tasks in the construction field, to name a few (1). Various aerial manipulation concepts have been proposed in the literature (2), but lightweight manipulation tools such as simple low-cost cables have often been preferred (3). Not only they are especially suitable due to the flying carriers' payload limitations, but, if attached ideally to the carrier's Center of Mass (CoM), they do not perturb the attitude dynamics of the carrier itself.

When disregarding the full-pose control of the suspended load, a single carrier may be considered. In the literature, we find examples of a slung load suspended below a single multirotor (4, 5) or a small helicopter (6).

Cooperative aerial manipulation allows for going beyond the single-carrier payload and avoids single points of failure. Among the examples of cooperative aerial manipulation with cables as manipulation tools, uncrewed helicopters have been used in (7), while multirotor UAVs (Uncrewed Aerial Vehicles) have been more generally considered (8–13). The two-multirotor scenario has been largely studied, especially for the manipulation of bar-shaped loads (14–16). However, three is the minimum number of carriers that can control the

full pose of a cable-suspended generic rigid body (17); such a 3-carrier system has been studied, e.g., in (8, 10, 18, 19).

As it has been shown, e.g., in (20), fixed-wing UAVs have a longer flight endurance than multirotor UAVs. However, they are constrained not to stop in mid-air. Furthermore, these platforms are unable to Vertical Take Off and Land (VTOL). Convertible UAVs such as tail sitters have an intermediate flight endurance. They have the feature of transitioning between VTOL platforms into fixed-wing ones, so as to exploit the benefit of the latter and multirotors, as well. An example of such a design is in proposed (20). Note that, when flying horizontally, also these platforms are constrained to follow non-stop trajectories.

Exploring the compatibility of non-stop flights with cable manipulation tasks could lead to a groundbreaking class of cable-suspended aerial systems. These systems would enable energy-efficient aerial manipulation, seamlessly integrating

¹Robotics and Mechatronics Department, Electrical Engineering, Mathematics, and Computer Science (EEMCS) Faculty, University of Twente, 7500 AE Enschede, The Netherlands.

²Department of Computer, Control and Management Engineering, Sapienza University of Rome, 00185 Rome, Italy.

Corresponding author:

Antonio Franchi, a.franchi@utwente.nl

long-distance transport with precise control of the load's pose.

This work focuses on maintaining a constant load pose while the carriers move, a scenario significantly more challenging than allowing the load to move as well. Moreover, ensuring a fixed load pose during transportation is critical in many practical situations, such as at the destination, or to enhance obstacle avoidance and safety. An abstract depiction of the future scenario made possible by this research is illustrated in Fig. 1.

The non-stop flight dynamics of the carriers make it challenging to determine whether they can hold a suspended load in static equilibrium while all loitering with a nonzero forward speed. In previous conference work (21), we presented preliminary results demonstrating the theoretical feasibility of three UAVs achieving this task, while establishing the impossibility of achieving it with only one or two carriers. However, the general case involving an arbitrary number of carriers remained unresolved. The proof presented in (21) was specifically tailored to the three-UAV scenario and did not readily extend to more general cases. Consequently, (21) left unanswered the fundamental question of whether non-stop flights are compatible with cable manipulation in the general case of multiple UAVs. Moreover, the preliminary work in (21) lacked a flexible algorithm for constructing feasible trajectories.

This work constitutes a substantial leap forward beyond the minimal findings of (21) by introducing the first method for generating non-stop flight trajectories for any $n \geq 3$ flying carriers. This method enables the carriers to maintain a cable-suspended load in static equilibrium while simultaneously executing their respective non-stop flight paths. This work also provides the first proof of the existence of such trajectories for any $n \geq 3$, as extending the results of (21) to the case of $n > 3$ is non-trivial. The introduction of a novel methodology, based on the selection of Hamiltonian cycles in the graph associated with the manipulation system, was crucial. This work also reformulates the theoretical framework using graph theory, resulting in a more general and rigorous approach. Furthermore, this work presents the first complete algorithm for generating compatible trajectories, along with guidelines for tuning the trajectory's free parameters to optimize performance based on the unique capabilities of each UAV. Finally, this work provides comprehensive validation of the theoretical findings through extensive numerical simulations.

The work is organized as follows. First, in Sec. , we introduce the notation and formalize the problem. Hence, in Sec. , we formally derive a method to generate non-stop trajectories for $n \geq 3$ flying carriers. To the best of the authors' knowledge, this is the first time such a problem is addressed for the general case of $n > 3$ carriers. In Sec. we present the full algorithm in a compact and implementable way and we provide qualitative remarks on the choice of

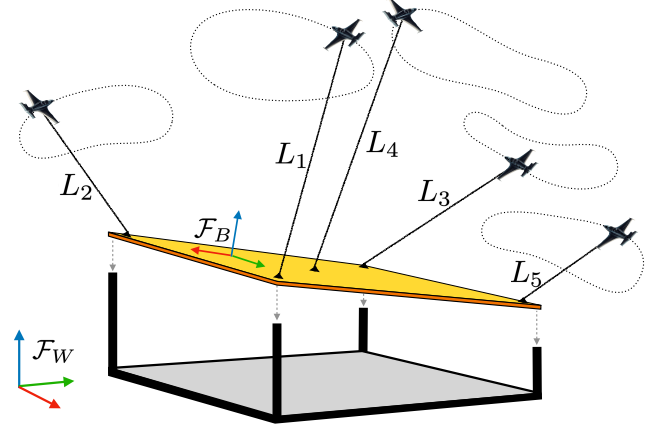


Figure 1. A team of $n \geq 3$ non-stop flying carriers maintains a cable-suspended load in a fixed position to enable a potential construction scenario, while all carriers continue on their respective non-zero speed flight paths

parameters. In Sec. , we show numerical results supporting the theoretical findings. Eventually, conclusions are drawn in Sec. together with an outline of future work.

Problem Statement

Kinematics

Denote with $\mathcal{F}_W = \{O_W, \mathbf{x}_W, \mathbf{y}_W, \mathbf{z}_W\}$, the inertial world-fixed frame where O_W is the origin, and $\mathbf{x}_W, \mathbf{y}_W, \mathbf{z}_W$ are the x-, y-, and z- axes, respectively, see Fig. 1. Denote with $\mathcal{F}_B = \{O_B, \mathbf{x}_B, \mathbf{y}_B, \mathbf{z}_B\}$ a frame attached to the manipulated load, modeled as a rigid body, where O_B is the Center of Mass (CoM) of the load. The position of O_B in \mathcal{F}_W is denoted with $\mathbf{p}_L \in \mathbb{R}^3$ and $\mathbf{R}_L \in SO(3)$ expresses the orientation of \mathcal{F}_B w.r.t. \mathcal{F}_W . The angular velocity of \mathcal{F}_B w.r.t. \mathcal{F}_W , expressed in \mathcal{F}_B is indicated as ${}^B\boldsymbol{\omega}_L^*$.

The load is manipulated by the flying carriers through n cables, each one of constant length $L_i > 0$

$$L_1 > 0L_2 > 0L_3 > 0L_4 > 0L_5 > 0L_3 > 0$$

and attached to a point B_i on the load and a point C_i to the carrier, with $i = 1, \dots, n$. Denote with ${}^B\mathbf{b}_i \in \mathbb{R}^3$ the constant position of B_i expressed in \mathcal{F}_B and with $\mathbf{p}_{Ri} \in \mathbb{R}^3$ the position of C_i in \mathcal{F}_W . Let the unit vector $\mathbf{q}_i \in S^2 = \{\mathbf{x} \in \mathbb{R}^3 \mid \|\mathbf{x}\| = 1\}$ pointing from B_i to C_i represent the direction of the i -th cable in \mathcal{F}_W . The kinematics of the points C_i 's is given by

$$\mathbf{p}_{Ri} = \mathbf{p}_L + \mathbf{R}_L {}^B\mathbf{b}_i + L_i \mathbf{q}_i \quad (1)$$

$$\dot{\mathbf{p}}_{Ri} = \dot{\mathbf{p}}_L + \dot{\mathbf{R}}_L {}^B\mathbf{b}_i + L_i \dot{\mathbf{q}}_i. \quad (2)$$

with $i = 1, \dots, n$.

*The upper left superscript expresses the reference frame, and if omitted it is considered equal to W unless differently specified.

Dynamics

The cables' mass and inertia are considered negligible compared to the carriers' and load's ones. This is a reasonable assumption which has been validated in practice (14, 22).

Denote with $T_i \in \mathbb{R}$ the tension of the i -th cable, where $i = 1, \dots, n$, and with \mathbf{f}_i the coordinates in \mathcal{F}_W of the force that the i -th cable exerts on the load at B_i . We have the following basic relation between the force, the cable direction, and the tension:

$$\mathbf{f}_i = T_i \mathbf{q}_i. \quad (3)$$

The dynamics of the load is described by

$$m_L \ddot{\mathbf{p}}_L = -m_L g \mathbf{e}_3 + \sum_{i=1}^n \mathbf{f}_i \quad (4)$$

$$\mathbf{J}_L^B \dot{\boldsymbol{\omega}}_L = -S(\mathbf{J}_L^B \boldsymbol{\omega}_L)^B \boldsymbol{\omega}_L + \sum_{i=1}^n S({}^B \mathbf{b}_i) \mathbf{R}_L^\top \mathbf{f}_i \quad (5)$$

$$\dot{\mathbf{R}}_L = S({}^B \boldsymbol{\omega}_L) \mathbf{R}_L \quad (6)$$

where m_L , \mathbf{J}_L are the mass and the rotational inertia of the load, $S(\star)$ indicates the skew operator that implements the cross product between two vectors, and \mathbf{e}_i is the i -th column of the 3×3 identity matrix \mathbf{I}_3 .

To compactly rewrite the load dynamics we use the matrix $\mathbf{G} \in \mathbb{R}^{6 \times 3n}$ that maps the cable forces to the wrench applied at the load's center of mass, referred to as grasp matrix in the literature (23, 24)

$$\mathbf{G} = \begin{bmatrix} \mathbf{I}_3 & \mathbf{I}_3 & \dots & \mathbf{I}_3 \\ S({}^B \mathbf{b}_1) \mathbf{R}_L^\top & S({}^B \mathbf{b}_2) \mathbf{R}_L^\top & \dots & S({}^B \mathbf{b}_n) \mathbf{R}_L^\top \end{bmatrix}. \quad (7)$$

The load dynamics (4)–(5) can be compactly rewritten as

$$\mathbf{w} := \begin{bmatrix} m_L (\ddot{\mathbf{p}}_L + g \mathbf{e}_3) \\ \mathbf{J}_L^B \dot{\boldsymbol{\omega}}_L + \mathbf{J}_L^B \boldsymbol{\omega}_L \times {}^B \boldsymbol{\omega}_L \end{bmatrix} = \mathbf{G} \mathbf{f} \quad (8)$$

where $\mathbf{f} = [\mathbf{f}_1^\top \ \mathbf{f}_2^\top \ \dots \ \mathbf{f}_n^\top]^\top \in \mathbb{R}^{3n}$ stacks all forces that the cables apply to the load and $\mathbf{w} \in \mathbb{R}^6$ represents the coordinates of the resulting wrench applied by the all cables on the load.

Statics

Consider a static equilibrium of the suspended load characterized by constant position $\bar{\mathbf{p}}_L$ and orientation $\bar{\mathbf{R}}_L$, i.e.,

$$\begin{cases} \mathbf{p}_L(t) = \bar{\mathbf{p}}_L \\ \mathbf{R}_L(t) = \bar{\mathbf{R}}_L \end{cases} \quad \forall t \in [0, \infty). \quad (9)$$

Imposing (9) on (8) and (1)–(2) and highlighting the time-varying quantities we obtain

$$\mathbf{w}_0 := \begin{bmatrix} m_L g \mathbf{e}_3 \\ \mathbf{0} \end{bmatrix} = \mathbf{G}(\bar{\mathbf{R}}_L) \mathbf{f}(t) \quad (10)$$

$$\mathbf{p}_{Ri}(t) = \bar{\mathbf{p}}_L + \bar{\mathbf{R}}_L^B \mathbf{b}_i + L_i \mathbf{q}_i(t) \quad \forall i = 1, \dots, n \quad (11)$$

$$\dot{\mathbf{p}}_{Ri}(t) = L_i \dot{\mathbf{q}}_i(t) \quad \forall i = 1, \dots, n. \quad (12)$$

If \mathbf{f}_i is of class C^1 (i.e., it is at least continuously differentiable) then we can differentiate (3) with respect to time obtaining

$$\dot{\mathbf{f}}_i(t) = \dot{T}_i(t) \mathbf{q}_i(t) + T_i(t) \dot{\mathbf{q}}_i(t). \quad (13)$$

If $T_i(t) = \|\mathbf{f}_i(t)\| \neq 0$, $\forall t \in [0, \infty)$, then $\mathbf{q}_i(t)$ and $\dot{\mathbf{q}}_i(t)$ can be derived from $\mathbf{f}_i(t)$, using (3) and (13) respectively. Substituting the obtained $\mathbf{q}_i(t)$ and $\dot{\mathbf{q}}_i(t)$ into (11)–(12), one can compute $\mathbf{p}_{Ri}(t)$ and $\dot{\mathbf{p}}_{Ri}(t)$. This demonstrates the intuitive idea that in static equilibrium—where the load's position and orientation remain constant over time—knowledge of the force trajectories is sufficient to determine how $\mathbf{p}_{Ri}(t)$ and $\dot{\mathbf{p}}_{Ri}(t)$ evolve over time. Consequently, it is reasonable to formulate the following problem.

Problem Coordinated Trajectories for Non-stop Flying Carriers Holding a Cable-Suspended Load. *Assume that the load is held at a constant position and orientation defined by (9). Find, if it exists, a coordinated trajectory of all the forces*

$$\mathbf{f}_i : [0, \infty) \rightarrow \mathbb{R}^3 \quad \forall i = 1, \dots, n \quad (14)$$

which satisfies the following conditions, for $i = 1, \dots, n$

- they are of class C^1 (at least continuously differentiable),
- they respect the equilibrium constraint (10) for the constant orientation, i.e.,

$$\mathbf{G}(\bar{\mathbf{R}}_L) \mathbf{f}(t) = \mathbf{w}_0 \quad \forall t \in [0, \infty), \quad (15)$$

where $\mathbf{f}(t) = [\mathbf{f}_1^\top(t) \ \dots \ \mathbf{f}_n^\top(t)]^\top$,

- they don't vanish and do not grow unbounded, i.e., $\exists \underline{T} > 0$ and $\exists \bar{T} < \infty$ such that the cable tension $T_i(t) = \|\mathbf{f}_i(t)\|$ satisfies

$$\underline{T} < T_i(t) < \bar{T} \quad \forall t \in [0, \infty), \quad (16)$$

and, finally, such that the carriers are never stopping and the norm of their velocity is lower bounded by a non-zero speed, i.e., for which $\exists \underline{v} > 0$ such that

$$\|\dot{\mathbf{p}}_{Ri}(t)\| \geq \underline{v}, \quad \forall t \in [0, \infty). \quad (17)$$

Formal Derivation of the Proposed Methodology

We know from (21) that the problem is not solvable for $n < 3$, and that there is a way to solve it in the particular case of $n = 3$. Therefore, in the following, we aim at solving the general problem for $n \geq 3$. Any coordinated trajectory of the collective forces that maintains the equilibrium is given by the following generic solution of (10)

$$\mathbf{f}(t) = \mathbf{G}^\dagger \mathbf{w}_0 + \mathbf{N} \boldsymbol{\lambda}(t) \quad (18)$$

where $\mathbf{G}^\dagger \in \mathbb{R}^{3n \times 6}$ is the Moore-Penrose inverse of $\mathbf{G}(\bar{\mathbf{R}}_L)$, \mathbf{N} is any constant matrix with m columns which are linearly independent and belong to $\text{null}(\mathbf{G})$, and $\boldsymbol{\lambda} : [0, \infty)^m \rightarrow \mathbb{R}^m$ is an array of time-varying coefficients $\boldsymbol{\lambda}(t) = [\lambda_1(t) \cdots \lambda_m(t)]^\top$ for the linear combination of the columns of \mathbf{N} expressed by $\mathbf{N}\boldsymbol{\lambda}(t)$. In our proposed method, we choose the matrix \mathbf{N} as described in Sec. , which necessitates the following graph preliminaries.

Preliminaries on Hamiltonian Cycles

Consider any directed Hamiltonian cycle H of the complete graph with n vertexes. The cycle H is composed of a loop of n edges connecting one after the other all the n vertexes and coming back to the starting vertex. Denote with $\mathbf{H} \in \{0, 1, -1\}^{n \times n}$ the incidence matrix of H . Denote the list of consecutive edges of H with e_1, \dots, e_n, e_{n+1} , where $e_{n+1} := e_1$ is introduced for convenience. Denote with e_i^1 and e_i^2 the index of the first and the second vertex of e_i , respectively, i.e., if $e_i = (j, k)$ then $e_i^1 = j$ and $e_i^2 = k$. Denote with h_i the index of the edge of H incoming to the vertex i , and consequently, $h_i + 1$ represents the index of the edge of H outgoing from the vertex i . This is due to the way the edges of H are indexed, see before. For example if $e_l = (*, i)$ then $h_i = l$ and $e_{h_i+1} = (i, *)$, where $*$ stands for an unspecified vertex number.

Example 1. For example, if $n = 4$ and H is the cycle that connects cyclically the vertexes with indexes $1 \rightarrow 3 \rightarrow 4 \rightarrow 2 \rightarrow 1$ in such order. We have $e_1 = (1, 3)$, $e_2 = (3, 4)$, $e_3 = (4, 2)$, $e_4 = (2, 1)$, $e_5 = e_1 = (1, 3)$. Additionally, for example, $e_1^1 = 1$, $e_2^1 = 3$, $e_3^1 = 4$, $e_4^1 = 1$, and so on; and $h_1 = 4$, $h_1 + 1 = 1$, $h_3 + 1 = 2$, $h_4 = 2$, $h_2 + 1 = 4$, and so on. The incidence matrix in this case is $\mathbf{H} = \begin{bmatrix} 1 & 0 & 0 & -1 \\ 0 & 0 & -1 & 1 \\ -1 & 1 & 0 & 0 \\ 0 & -1 & 1 & 0 \end{bmatrix}$, where the i -th column corresponds to the edge e_i and the j -th row corresponds to the vertex j .

Remark 1. Notice the structure of the square matrix \mathbf{H} :

- the i -th column (which represents the edge e_i) has a 1 corresponding to the e_i^1 -th row, a -1 corresponding to the e_i^2 -th row, and the rest $n - 2$ entries are all zero's;
- the i -th row (which represents the vertex i) has a -1 corresponding to the h_i -th column, a 1 corresponding to the $h_i + 1$ -th column, and the rest $n - 2$ entries are all zero's.

Decision of the null-space matrix \mathbf{N}

Define the vector $\mathbf{b}_{ij} \in \mathbb{R}^3$ as follows:

$$\mathbf{b}_{ij} := \bar{\mathbf{R}}_L(\mathbf{B}\mathbf{b}_j - \mathbf{B}\mathbf{b}_i)$$

for any $i, j \in \{1, \dots, n\}$. Notice that $\mathbf{b}_{ij} = -\mathbf{b}_{ji}$. After arbitrarily selecting one of the Hamiltonian cycles of the complete graph with n vertexes, the matrix \mathbf{N} is defined as

a $3n \times n$ matrix as follows:

$$\mathbf{N}(H) = (\mathbf{H} \otimes \mathbf{I}_3) \cdot \text{diag}(\mathbf{b}_{e_1^1 e_1^2}, \dots, \mathbf{b}_{e_n^1 e_n^2}), \quad (19)$$

where \otimes denotes the Kronecker product and diag denotes a block diagonal matrix.[†]

Example 2. With reference to the Example 1 we have

$$\text{diag}(\mathbf{b}_{e_1^1 e_1^2}, \dots, \mathbf{b}_{e_n^1 e_n^2}) = \begin{bmatrix} \mathbf{b}_{13} & \mathbf{0} & \mathbf{0} & \mathbf{0} \\ \mathbf{0} & \mathbf{b}_{34} & \mathbf{0} & \mathbf{0} \\ \mathbf{0} & \mathbf{0} & \mathbf{b}_{42} & \mathbf{0} \\ \mathbf{0} & \mathbf{0} & \mathbf{0} & \mathbf{b}_{21} \end{bmatrix} \in \mathbb{R}^{12 \times 4}.$$

$$\mathbf{N}(H) = \begin{bmatrix} \mathbf{b}_{13} & \mathbf{0} & \mathbf{0} & -\mathbf{b}_{21} \\ \mathbf{0} & \mathbf{0} & -\mathbf{b}_{42} & \mathbf{b}_{21} \\ -\mathbf{b}_{13} & \mathbf{b}_{34} & \mathbf{0} & \mathbf{0} \\ \mathbf{0} & -\mathbf{b}_{34} & \mathbf{b}_{42} & \mathbf{0} \end{bmatrix} \in \mathbb{R}^{12 \times 4}.$$

For simplicity, in the following, we omit the dependency of \mathbf{N} on the particular H when the choice of H is either implicit or non-discriminatory.

We can easily check that the i -th column of the chosen \mathbf{N} , denoted with $\mathbf{N}_{(:,i)}$, belongs to $\text{null}(\mathbf{G})$, in fact:

$$\begin{aligned} \mathbf{G}\mathbf{N}_{(:,i)} &= \begin{bmatrix} \mathbf{b}_{e_i^1 e_i^2} - \mathbf{b}_{e_i^1 e_i^2} \\ S(\mathbf{B}\mathbf{b}_{e_i^1})\mathbf{R}_L^\top \mathbf{b}_{e_i^1 e_i^2} - S(\mathbf{B}\mathbf{b}_{e_i^2})\mathbf{R}_L^\top \mathbf{b}_{e_i^1 e_i^2} \end{bmatrix} = \\ &= \begin{bmatrix} \mathbf{0} \\ S(\mathbf{B}\mathbf{b}_{e_i^1})(\mathbf{B}\mathbf{b}_{e_i^2} - \mathbf{B}\mathbf{b}_{e_i^1}) - S(\mathbf{B}\mathbf{b}_{e_i^2})(\mathbf{B}\mathbf{b}_{e_i^2} - \mathbf{B}\mathbf{b}_{e_i^1}) \end{bmatrix} = \\ &= \begin{bmatrix} \mathbf{0} \\ S(\mathbf{B}\mathbf{b}_{e_i^1})\mathbf{B}\mathbf{b}_{e_i^2} + S(\mathbf{B}\mathbf{b}_{e_i^2})\mathbf{B}\mathbf{b}_{e_i^1} \end{bmatrix} = \begin{bmatrix} \mathbf{0} \\ \mathbf{0} \end{bmatrix}, \end{aligned}$$

where we exploited the fact that $S(\mathbf{x})\mathbf{x} = \mathbf{0}$ and $S(\mathbf{x}_1)\mathbf{x}_2 = -S(\mathbf{x}_2)\mathbf{x}_1$ for any $\mathbf{x}, \mathbf{x}_1, \mathbf{x}_2 \in \mathbb{R}^3$.

Force of the i -th cable for the chosen \mathbf{N}

From (18), the force applied by the i -th cable is expressed as

$$\mathbf{f}_i(t) = \mathbf{f}_{0i} + \mathbf{N}_i \boldsymbol{\lambda}(t)$$

where $\mathbf{f}_{0i} \in \mathbb{R}^3$ is the vector obtained by the three components of $\mathbf{G}^\dagger \mathbf{w}_0$ at the positions $3(i-1) + \{1, 2, 3\}$, and $\mathbf{N}_i \in \mathbb{R}^{3 \times n}$ is made by the 3 rows of \mathbf{N} located at the same positions, which induces the following block partition $\mathbf{N} = [\mathbf{N}_1^\top \cdots \mathbf{N}_n^\top]^\top$.

Using the definition of h_i and $h_i + 1$ and remembering what said in Remark 1 regarding the rows of \mathbf{H} , we have that

$$\mathbf{N}_i \boldsymbol{\lambda}(t) = -\lambda_{h_i}(t) \mathbf{b}_{e_{(h_i)}^1 e_{(h_i)}^2} + \lambda_{h_i+1}(t) \mathbf{b}_{e_{(h_i+1)}^1 e_{(h_i+1)}^2}.$$

For the sake of brevity, we define $\boldsymbol{\delta}_i := -\mathbf{b}_{e_{h_i}^1 e_{h_i}^2}$, $\bar{\boldsymbol{\delta}}_i := \mathbf{b}_{e_{h_i+1}^1 e_{h_i+1}^2}$, $\mu_i(t) := \lambda_{h_i}(t)$, and $\bar{\mu}_i(t) := \lambda_{h_i+1}(t)$. Thus we can rewrite the previous equation as

$$\mathbf{N}_i \boldsymbol{\lambda}(t) = \mu_i(t) \boldsymbol{\delta}_i + \bar{\mu}_i(t) \bar{\boldsymbol{\delta}}_i. \quad (20)$$

[†]For the sake of completeness we note that the matrix $\mathbf{N}(H)$ is the transposed of the Rigidity matrix associated to the framework $(H, (\mathbf{p}_{R1}, \dots, \mathbf{p}_{Rn}))$, see e.g., (25) for a definition.

Assumption 1. *Corresponding to the selected Hamiltonian cycle, we have that for any $i = 1, \dots, n$, the three attachment points B_i , $B_{e_{h_i}^1}$ and $B_{e_{h_i+1}^2}$ are not aligned, or equivalently, the vectors ${}^B\mathbf{b}_i - {}^B\mathbf{b}_{e_{h_i}^1}$ and ${}^B\mathbf{b}_{e_{h_i+1}^2} - {}^B\mathbf{b}_i$ are linearly independent.*

Assumption 1 ensures that for any $i = 1, \dots, n$ the vectors δ_i and $\bar{\delta}_i$ are not parallel and therefore

- $\text{span}\{\delta_i, \bar{\delta}_i\}$ is a 2D subspace of \mathbb{R}^3 , and
- $\text{rank}(\mathbf{N}) = n$, i.e., all the columns of \mathbf{N} are linearly independent.

To assess the truth of the second statement, consider that for all $i = 1, \dots, n$, we have $\mathbf{N}_i \boldsymbol{\lambda} = \mathbf{0}$ if and only if both $\mu_i = 0$ and $\bar{\mu}_i = 0$, see (20). Therefore, the only $\boldsymbol{\lambda} \in \mathbb{R}^n$ which makes $\mathbf{N}\boldsymbol{\lambda} = \mathbf{0}$ is $\boldsymbol{\lambda} = \mathbf{0}$.

We can then recap the main results obtained so far in the following statement.

Result 1. *After arbitrarily selecting one of the Hamiltonian cycles of the complete graph with n vertices, construct a matrix $\mathbf{N}(H) \in \mathbb{R}^{3n \times n}$ as described in (19). If Assumption 1 is valid, then:*

- the n columns of \mathbf{N} belong to the nullspace of \mathbf{G} and are linearly independent.
- The force applied by the i -th carrier has the following affine structure:

$$\mathbf{f}_i(t) = \mathbf{f}_{0i} + \underbrace{\mu_i(t) \delta_i + \bar{\mu}_i(t) \bar{\delta}_i}_{=: \bar{\mathbf{f}}_i(t) \in \text{span}\{\delta_i, \bar{\delta}_i\}}. \quad (21)$$

This expression shows that at any time t , $\mathbf{f}_i(t)$ lies in the affine 2D subspace of \mathbb{R}^3 that passes through \mathbf{f}_{0i} and is parallel to $\text{span}\{\delta_i, \bar{\delta}_i\}$. The quantities $\mu_i(t)$ and $\bar{\mu}_i(t)$ represent the coordinates of the projection of $\mathbf{f}_i(t)$ along $-\mathbf{f}_{0i}$ onto this subspace w.r.t. δ_i and $\bar{\delta}_i$, respectively (see Fig. 2).

- The time derivative of the force is given by

$$\dot{\mathbf{f}}_i(t) = \dot{\mu}_i(t) \delta_i + \dot{\bar{\mu}}_i(t) \bar{\delta}_i, \quad (22)$$

which means that $\dot{\mathbf{f}}_i(t)$ lies in the 2D subspace of \mathbb{R}^3 spanned by $\delta_i, \bar{\delta}_i$. The quantities $\dot{\mu}_i(t)$ and $\dot{\bar{\mu}}_i(t)$ represent the coordinates of $\dot{\mathbf{f}}_i(t)$ in this subspace along δ_i and $\bar{\delta}_i$, respectively.

Relation between force derivative and carrier velocity

So far, we have seen how the particular choice of \mathbf{N} simplifies the evolution of the force applied by the i -th cable and its time derivative, by restricting the latter to evolve within a 2D subspace, and the former to evolve within a parallel 2D affine subspace passing through \mathbf{f}_{0i} .

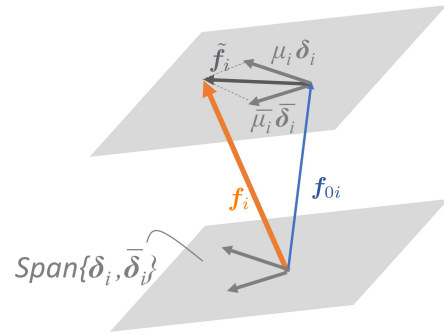


Figure 2. Geometric visualization of the force of the i -th carrier and its components.

Remark 2. Notice the fact that with this choice the n forces belong to n different 2D affine subspaces despite the fact that the attachment points are in general distributed in 3D.

In this section, we will explore how this result is instrumental in drawing important consequences for relating the time derivative of the force to the velocity of the i -th carrier.

Starting from and further analyzing (13) the time derivative of the i -cable force is given by

$$\dot{\mathbf{f}}_i = \dot{T}_i \mathbf{q}_i + T_i \dot{\mathbf{q}}_i = \dot{\mathbf{f}}_i^{\parallel} + \dot{\mathbf{f}}_i^{\perp}$$

where $\dot{\mathbf{f}}_i^{\parallel} = \dot{T}_i \mathbf{q}_i$ represents the change along the direction parallel to the one of the force, i.e., the change of the force intensity, and $\dot{\mathbf{f}}_i^{\perp} = T_i \dot{\mathbf{q}}_i$ represents the change orthogonal to the force, i.e., the change of the force direction.

Recalling (12), we have in general the following

Result 2. *With the assumption of static load, and as long as the tension on the i -th cable T_i is positive and bounded,*

- the velocity of the i -th carrier is collinear and proportional to $\dot{\mathbf{f}}_i^{\perp}$ through the following relation

$$\dot{\mathbf{p}}_{Ri}(t) = \frac{T_i}{T_i(t)} \dot{\mathbf{f}}_i^{\perp}(t). \quad (23)$$

- The velocity of the i -th carrier $\dot{\mathbf{p}}_{Ri}(t)$ is nonzero as long as the direction of the force changes, i.e., as long as $\dot{\mathbf{f}}_i^{\perp}(t)$ is nonzero.

We can now state the main result of this section which is a consequence of our particular choice of \mathbf{N} as an $\mathbf{N}(H)$ for a Hamiltonian cycle H .

Lemma 1. *After arbitrarily selecting one of the Hamiltonian cycles of the complete graph with n vertices, denoted with H , construct a matrix $\mathbf{N}(H) \in \mathbb{R}^{3n \times n}$ as described in (19). Then, the following conditions are sufficient to have $\|\dot{\mathbf{p}}_{Ri}(t)\| > 0$*

1. Assumption 1 holds,
2. $\mathbf{f}_{0i} \notin \text{span}\{\delta_i, \bar{\delta}_i\}$,

3. $\mu_i(t)$ and $\bar{\mu}_i(t)$ are bounded,

4. $|\dot{\bar{\mu}}_i(t)| + |\dot{\mu}_i(t)| \neq 0$.

Proof. The assumptions of Result 2 are satisfied because of the following two facts:

- since $\mathbf{f}_{0i} \notin \text{span}\{\bar{\delta}_i, \delta_i\}$ the affine 2D subspace where $\mathbf{f}_i(t)$ belongs to does not pass through the origin and therefore $\mathbf{f}_i(t)$ is nonzero for any t and so is $T_i(t)$.
- Since $\mu_i(t)$ and $\bar{\mu}_i(t)$ are bounded then $\|\mathbf{f}_i(t)\|$ is bounded and so is $T_i(t)$.

From Result 2 we know that in order to show that $\|\dot{\mathbf{p}}_{Ri}(t)\| > 0$ it is enough to show that $\|\dot{\mathbf{f}}_i^\perp(t)\| > 0$, and we do this by showing the next two points

- (non vanishing derivative) $\|\dot{\mathbf{f}}_i(t)\| \neq 0$, and
- (non-collinear force and derivative) $\dot{\mathbf{f}}_i(t)$ is not collinear with $\mathbf{f}_i(t)$.

Non vanishing From $|\dot{\bar{\mu}}_i(t)| + |\dot{\mu}_i(t)| \neq 0$ it follows that $\dot{\bar{\mu}}_i(t)$ and $\dot{\mu}_i(t)$ are not simultaneously zero and therefore $\|\dot{\mathbf{f}}_i(t)\| \neq 0$.

Non-collinear. By contradiction assume that $\mathbf{f}_i(t)$ is collinear with $\dot{\mathbf{f}}_i(t)$, therefore also their sum

$$\dot{\mathbf{f}}_i(t) + \mathbf{f}_i(t) = \mathbf{f}_{0i} + \tilde{\mathbf{f}}_i(t) + \mathbf{f}_i(t)$$

is collinear with $\dot{\mathbf{f}}_i(t)$, and therefore their sum is contained in $\text{span}\{\delta_i, \bar{\delta}_i\}$. However on the right hand side of the previous equation, $\tilde{\mathbf{f}}_i(t) + \mathbf{f}_i(t)$ is contained in $\text{span}\{\delta_i, \bar{\delta}_i\}$ while $\mathbf{f}_{0i} \notin \text{span}\{\delta_i, \bar{\delta}_i\}$, which implies that the sum is not contained in $\text{span}\{\delta_i, \bar{\delta}_i\}$, which brings to the sought contradiction.

We have shown that the assumptions of Result 2 are satisfied and so the proposition is proven by applying the second point in Result 2.

Decision of the time-varying coefficients $\lambda(t)$

In Lemma 1, we have seen that two important conditions to be satisfied are that, for every carrier $i = 1, \dots, n$,

- $\mu_i(t)$ and $\bar{\mu}_i(t)$ are bounded, and
- $|\dot{\bar{\mu}}_i(t)| + |\dot{\mu}_i(t)| \neq 0$, i.e., $\dot{\bar{\mu}}_i$ and $\dot{\mu}_i$ are not simultaneously zero.

In order to satisfy the first condition it is enough to chose smooth bounded functions for the $\lambda_i(t)$'s, for example, a natural choice is to choose periodic functions which oscillate between a maximum and a minimum, as, e.g., the combination of some trigonometric functions of time.

Restating the second condition for the original $\lambda_i(t)$'s variables, we see that for the second condition, we must guarantee that $\lambda_i(t)$ and $\lambda_{i+1}(t)$ are not simultaneously zero for all $i = 1, \dots, n$ (with $\lambda_{n+1} := \lambda_1$). Since in order to satisfy the boundedness condition we have opted for smooth

oscillatory functions, we need to choose carefully those functions such that the pair $\lambda_i(t)$ and $\lambda_{i+1}(t)$ do not attain their stationary points simultaneously, for every consecutive pair of edges obtained when $i = 1, \dots, n$.

Assume that we define a finite library C of periodical functions of time which do not have any simultaneous stationary point in common, denote such library with $C = \{c_1(t), c_2(t), \dots, c_{n_c}(t)\}$. Formally, we are imposing that $\{t \in \mathbb{R} \mid \dot{c}_i(t) = 0\} \cap \{t \in \mathbb{R} \mid \dot{c}_j(t) = 0\} = \emptyset$ for every $i, j = 1, \dots, n_c$, with $j \neq i$.

The problem is then to assign to each edge of the Hamiltonian cycle H one function in C such that two incident (consecutive) edges, e_i and e_{i+1} , do not have the same function assigned. This is a type of problem called *edge coloring* in graph theory. The minimum number of colors for edge coloring in a cycle graph such as H is two if the number of edges is even and three if the number of edges is odd (26). Therefore, to account for any possible case, it is enough to have a library with three functions, e.g.,

$$\begin{aligned} c_1(t) &= A \cos(\xi t) \\ c_2(t) &= A \cos(\xi t + \frac{\pi}{3}) \\ c_3(t) &= A \cos(\xi t + \frac{2\pi}{3}) \end{aligned} \quad (24)$$

where $A > 0$ and $\xi > 0$ are any amplitude and angular frequency, respectively, and then equate each $\lambda_i(t)$ to one of such functions, taking care of avoiding that the same function is assigned both to $\lambda_i(t)$ and $\lambda_{i+1}(t)$ for any $i = 1, \dots, n$, with $\lambda_{n+1}(t) := \lambda_1(t)$. With this choice, and following an appropriate assignment corresponding to the coloring of H , we obtain that when $\dot{\lambda}_i(t) = 0$, it follows that $\dot{\lambda}_{i+1}(t) = \pm A\xi \frac{\sqrt{3}}{2}$. Therefore, by Lemma 1, we conclude that $\|\dot{\mathbf{p}}_{Ri}\| > 0$.

Of course, an infinite number of other choices are possible, e.g., in the case of an even number of carriers one could use a simplified library with just two functions out of phase by $\frac{\pi}{2}$ radians

$$\begin{aligned} c_1(t) &= A \cos(\xi t) \\ c_2(t) &= A \cos(\xi t + \frac{\pi}{2}). \end{aligned} \quad (25)$$

By assigning c_1 and c_2 alternatively to consecutive edges of H , we have that when $\dot{\lambda}_i(t) = 0$, then $\dot{\lambda}_{i+1}(t) = \pm A\xi$.

We can now state the conclusive result of this section.

Proposition 1. *After arbitrarily selecting one of the Hamiltonian cycles of the complete graph with n vertices, denoted with H construct a matrix $\mathbf{N}(H) \in \mathbb{R}^{3n \times n}$ as described in (19). Furthermore, assume that the following conditions are true:*

1. Assumption 1 holds,
2. $\mathbf{f}_{0i} \notin \text{span}\{\delta_i, \bar{\delta}_i\}$,
3. the $\lambda_i(t)$'s are chosen via edge coloring of the selected Hamiltonian cycle using as a library of functions (25)

for the case of an odd n or (24) for the case of an even n ,

then the Problem of Coordinated Trajectories for Non-stop Flying Carriers holding a Cable-Suspended Load is solved.

Proof. We will show that all the requirements of the Problem are met by the proposed choice of coordinated trajectories. Choosing $\lambda_i(t)$'s via edge coloring from the libraries (25) or (24) ensures that the forces (21) belong to class C^1 . Furthermore (15) holds thanks to (20). Additionally, the forces do not vanish for what is said in the proof of Lemma 1. Furthermore, for any bounded A in (25) or (24), the forces are upper-bounded because each force consists of a constant term and a variable term with bounded periodic coordinates. Therefore, (16) is satisfied.

Finally, the next part of the proof is aimed at showing that (17) holds. Combining (22) and the time derivatives of (25) or (24), we can write

$$\dot{\mathbf{f}}_i = [\delta_i \quad \bar{\delta}_i] \begin{bmatrix} \dot{\mu}_i \\ \dot{\mu}_i \end{bmatrix} = \quad (26)$$

$$= [\delta_i \quad \bar{\delta}_i] \xi A \begin{bmatrix} -\sin \beta_i & -\cos \beta_i \\ -\sin \bar{\beta}_i & -\cos \bar{\beta}_i \end{bmatrix} \begin{bmatrix} \cos(\xi t) \\ \sin(\xi t) \end{bmatrix} := \quad (27)$$

$$:= \xi \Delta_i \mathbf{M}_i(\beta_i, \bar{\beta}_i, A) \begin{bmatrix} \cos(\xi t) \\ \sin(\xi t) \end{bmatrix}, \quad (28)$$

where $\Delta_i := [\delta_i \quad \bar{\delta}_i]$, $\mathbf{M}_i := A \begin{bmatrix} -\sin \beta_i & -\cos \beta_i \\ -\sin \bar{\beta}_i & -\cos \bar{\beta}_i \end{bmatrix}$ where $\beta_i \in \{0, \pi/3, 2\pi/3\}$ and $\bar{\beta}_i \in \{0, \pi/3, 2\pi/3\}/\{\beta_i\}$ for an odd n (or $\beta_i \in \{0, \pi/2\}$ and $\bar{\beta}_i \in \{0, \pi/2\}/\{\beta_i\}$ for an even n) are the constant phases of the sinusoidal functions in (25), (24) corresponding to the two edges adjacent to the i -th vertex. Thanks to the edge coloring, the two constant phases are different; therefore, \mathbf{M}_i is full-rank. For Assumption 1, Δ_i is also full-rank. Hence, $\Delta_i \mathbf{M}_i \begin{bmatrix} \cos(\xi t) \\ \sin(\xi t) \end{bmatrix}$ is a parametrization of a 2D ellipses whose minor axis length is nonzero and is denoted with $\underline{\gamma}_i > 0$. In other words, for (28) we have that $\forall t, \|\dot{\mathbf{f}}_i\| \geq \xi \underline{\gamma}_i$. For the same argument used in Lemma 1, we know that \mathbf{f}_i and $\dot{\mathbf{f}}_i$ are not collinear, therefore we can state that for any non-zero $\dot{\mathbf{f}}_i$, there is a non-zero $\dot{\mathbf{f}}_i^\perp$. More specifically there exists $\alpha_i > 0$ such that $\|\dot{\mathbf{f}}_i^\perp\| \geq \alpha_i \|\dot{\mathbf{f}}_i\|$. Finally, we have that $\|\dot{\mathbf{f}}_i^\perp\| \geq \xi \alpha_i \underline{\gamma}_i$. Applying (23) we have that $\|\dot{\mathbf{p}}_{Ri}(t)\| \geq \frac{L_i}{T_i(t)} \xi \alpha_i \underline{\gamma}_i \geq \frac{L_i}{T_i} \xi \alpha_i \underline{\gamma}_i$. Finally, we can conclude that there exists

$$\underline{v} = \frac{L_i}{T_i} \xi \alpha_i \underline{\gamma}_i \quad (29)$$

such that $\forall t, \|\dot{\mathbf{p}}_{Ri}\| \geq \underline{v}$. Therefore all the requirements of the Problem are met by the proposed choice of coordinated trajectories. Note also that, with analogous reasoning and calling the major axis of the 2D ellipses $\bar{\gamma}_i$, we have $\|\dot{\mathbf{p}}_{Ri}(t)\| \leq \frac{L_i}{T_i(t)} \xi \alpha_i \bar{\gamma}_i \leq \frac{L_i}{T_i} \xi \alpha_i \bar{\gamma}_i$.

Algorithm 1 Computation of the non-stop carrier trajectories

```

 $[\mathbf{p}_{R1}, \dot{\mathbf{p}}_{R1}, \dots, \mathbf{p}_{Rn}, \dot{\mathbf{p}}_{Rn}] =$ 
compute_carrier_trajectories( $n, m_L, \bar{\mathbf{R}}_L, \bar{\mathbf{p}}_L, {}^B \mathbf{b}_1, \dots, {}^B \mathbf{b}_n$ )
    if  $n \notin \mathbb{N}$  or  $n < 3$  or  $m_L \leq 0$  or  ${}^B \mathbf{b}_i \notin \mathbb{R}^3$  then
        return error
    end if
     $\mathbf{G}(\bar{\mathbf{R}}_L, {}^B \mathbf{b}_i) \leftarrow (7)$ 
     $\mathbf{f}_0 \leftarrow \mathbf{G}^\dagger \begin{bmatrix} m_L \mathbf{g} e_3 \\ \mathbf{0}_{3 \times 1} \end{bmatrix}$ 
     $j \leftarrow 1, i \leftarrow 1$ 
    for  $i \leq n$  do
         $\mathbf{f}_{0i} \leftarrow \mathbf{f}_0(j : j + 2)$ 
         $j \leftarrow j + 3$ 
    end for
     $\triangleright$  Find a Hamiltonian cycle satisfying conditions 1) and 2)
of Proposition 1
 $\mathcal{H} \leftarrow$  all Hamiltonian cycles.
while TRUE do
     $h \leftarrow$  draw a cycle from  $\mathcal{H}$ 
     $\mathcal{H} \leftarrow \mathcal{H} \setminus h$ 
    for  $j \neq n$  do
         $\delta_i = \bar{\mathbf{R}}_L ({}^B \mathbf{b}_{e_{h_i}^2} - {}^B \mathbf{b}_{e_{h_i}^1})$ 
         $\bar{\delta}_i = \bar{\mathbf{R}}_L ({}^B \mathbf{b}_{e_{h_{i+1}}^2} - {}^B \mathbf{b}_{e_{h_{i+1}}^1})$ 
    end for
    if rank( $[\mathbf{f}_{0i} \quad \delta_i \quad \bar{\delta}_i]$ ) = 3, for all  $i = 1, \dots, n$  then
        Break
    end if
    if  $\mathcal{H} = \emptyset$  then
        return error
    end if
end while
 $\mathbf{H} \leftarrow$  incidence matrix of  $h$ 
 $\mathbf{N} \leftarrow (19)$ 
 $\triangleright$  Apply edge coloring using (25) or (24).

if  $n$  is even then
    for  $j \leq n - 2$  do  $\lambda_j(t) \leftarrow c_1(t)$  in (25)
         $\lambda_{j+1}(t) \leftarrow c_2(t)$  in (25)
         $j \leftarrow j + 2$ 
    end for
else
    for  $j \leq n - 3$  do  $\lambda_j(t) \leftarrow c_1(t)$  in (24)
         $\lambda_{j+1}(t) \leftarrow c_2(t)$  in (24)
         $\lambda_{j+2}(t) \leftarrow c_2(t)$  in (24)
         $j \leftarrow j + 3$ 
    end for
end if
 $\triangleright$  Compute the cable forces and use kinematics to compute
the carriers' trajectories
for  $j = 1 : n, \forall t > 0$  do
     $\mathbf{f}_j(t) \leftarrow (21)$ 
     $T_j \leftarrow \|\mathbf{f}_j\|$ 
     $\mathbf{q}_j \leftarrow \frac{\mathbf{f}_j}{T_j}$ 
     $\dot{\mathbf{f}}_j \leftarrow (22)$ 
     $\dot{\mathbf{q}}_j \leftarrow (\dot{\mathbf{f}}_j - \mathbf{q}_j \mathbf{q}_j^\top \dot{\mathbf{f}}_j) / T_j$ 
     $\mathbf{p}_{Rj} \leftarrow (11)$ 
     $\dot{\mathbf{p}}_{Rj} \leftarrow (12)$ 
end for

```

Algorithm and Qualitative Remarks

Algorithm to generate Coordinated Trajectories for Non-stop Flying Carriers Holding a Cable-Suspended Load

Algorithm 1 presents a conceptual pseudo-code of the solution formally derived in Sec. . This algorithm computes a set of n coordinated trajectories for the n carriers. These trajectories are periodic, never stopping, continuously differentiable, and ensure compatibility with the forces required to hold the load stationary.

Qualitative Remarks about the Choice of Free Parameters in the Algorithm

Remark 3. (Choice of the Hamiltonian cycle among the $\frac{(n-1)!}{2}$ possible for n carriers). There may be certain Hamiltonian cycles that are inadmissible because they would violate two of the assumptions of Proposition 1. First, there might exist Hamiltonian cycles for which Assumption 1 does not hold. In that case, $\text{span}\{\delta_i, \bar{\delta}_i\}$ is a 1D subspace of \mathbb{R}^3 , and $\nexists \lambda(t)$ such that $\|\dot{p}_{Ri}(t)\| \geq \underline{v}$ for $\underline{v} > 0$, as we showed in (21). Note that if there exist no three collinear cable attachment points on the load, then Assumption 1 holds for any Hamiltonian cycle.

Secondly, any Hamiltonian cycle for which $f_{0i} \in \text{span}\{\delta_i, \bar{\delta}_i\}$ is not admissible. That would imply that the total cable force $f_i(t)$, and hence $T_i(t)$, may be equal to zero. This invalidates our model in (23). Secondly, $f_{0i} \in \text{span}\{\delta_i, \bar{\delta}_i\}$ would allow $f_i(t)$ and $\dot{f}_i(t)$ to be collinear (see Proof of Lemma 1), and hence a variation of the force $f_i(t)$ (i.e., a non-zero $\dot{f}_i(t)$) would not necessarily imply a non-zero $\dot{p}_{Ri}(t)$.

From what has been said, we hypothesize that it is desirable to choose a Hamiltonian cycle for which δ_i and $\bar{\delta}_i$ are as much as possible orthogonal. In that way, the carrier's motion is as far as possible from being constrained on a 1D space (δ_i and $\bar{\delta}_i$ linearly dependent). Specifically, the 2D ellipses represented by (28) becomes more and more skew as δ_i and $\bar{\delta}_i$ are more aligned. Consequently, the minimum of the carriers' velocities \underline{v} in (29) is lower (with everything else remaining unchanged). Moreover, we hypothesize that it is better to choose Hamiltonian cycles such that f_{0i} is as much orthogonal as possible to $\text{span}\{\delta_i, \bar{\delta}_i\}$. In that way, we avoid that, even for large $\dot{\mu}_i$ and $\ddot{\mu}_i$, the value of α_i , and hence $\dot{f}_i^\perp(t)$, is small; that would result in a small minimum value $\underline{v}(\alpha_i)$ of \dot{p}_{Ri} (see (29)).

Remark 4. (Choice of the frequency ξ) From the proof of Proposition 1, we have that the minimum carriers' velocity \underline{v} can be increased at will by increasing the frequency ξ in (25), (24). Note that increasing instead the amplitude A would increase \bar{T} as well, thus defeating the purpose of increasing \underline{v} in (29).

Remark 5. (Choice of the library of periodic functions C) In Section , we gave a library of 2 (for n even) or 3 (for n odd) sinusoidal functions to assign to $\lambda_i(t)$. Note that a library of n functions $c_i(t) = A \cos(\xi t + \phi_i)$ for $i = 1, \dots, n$ with phases all spaced by π/n , namely $\phi_i = \frac{\pi}{n}(i-1)$, can be used to ensure that the same assignment of $\lambda_i(t)$ is valid for any possible Hamiltonian cycle. As a drawback, the phases $\lambda_i(t)$ paired together are closer to each other, leading to a larger eccentricity of the force derivative ellipses in the plane $\text{span}\{\delta_i, \bar{\delta}_i$ and hence to large force (and carrier velocity) variations. Note also that a library of different bounded periodic functions that do not simultaneously attain stationary points may be also used.

Numerical Results

In this section, we show simulation results that validate and reinforce the analysis discussed earlier.

The simulations have been carried out in Matlab-Simulink. Each flying carrier is simulated as a double integrator controlled via a PD feedback law to follow a desired trajectory. The carriers' mass is 0.1 kg, and the proportional and derivative gain matrices, making the carriers' dynamics overdamped, are diagonal matrices with values on the diagonal of 100 N/m and 10 Ns/m, respectively. To simulate sensor noise, a Gaussian random signal is added to the position and velocity of the carriers, with a standard deviation of 0.005 m and 0.01 m/s, respectively. The suspended rigid body load has a mass of 1 kg and diagonal rotational inertia with diagonal elements equal to 0.01 N-m/s. Viscous friction with a coefficient of 0.1 Ns/m is added to the load's translational and rotational dynamics to simulate friction with the air. The cables are hence modeled as linear springs with a rigidity of $K_c = 500$ N/m, damping coefficient $B_c = 1$ Ns/m and a rest length of 0.8 m. The load equilibrium configuration is chosen without loss of generality in $\bar{p}_L = [0, 0, 0]^T$, $\bar{R}_L = I_3$.

The role of the Hamiltonian cycle on the carriers' velocity

In this section, we empirically assess the effect of the specific Hamiltonian cycle selected on the carrier's velocity. We simulate a system with $n = 4$ evenly distributed cable attachment points around the center of mass, on a circumference of radius 1.2 m. In such a system, $\forall i = 1, \dots, 4$, f_{0i} is orthogonal to $\text{span}\{\delta_i, \bar{\delta}_i\}$. Of the 3 possible Hamiltonian cycles, there is one where $\forall i = 1, \dots, 4$, δ_i and $\bar{\delta}_i$ are orthogonal. For what has been discussed in Section , this should lead to a larger minimum of $\dot{p}_{Ri}(t)$ (and a larger maximum, as well). Indeed, as shown in the results reported in Figure 3, the minimum of the carriers' velocities is greater when choosing the first cycle than when selecting the other two. The choice of $\lambda_i(t)$ follows the coloring procedure in Section , with $A = 1$ N, $\xi = 2$ rad/s.

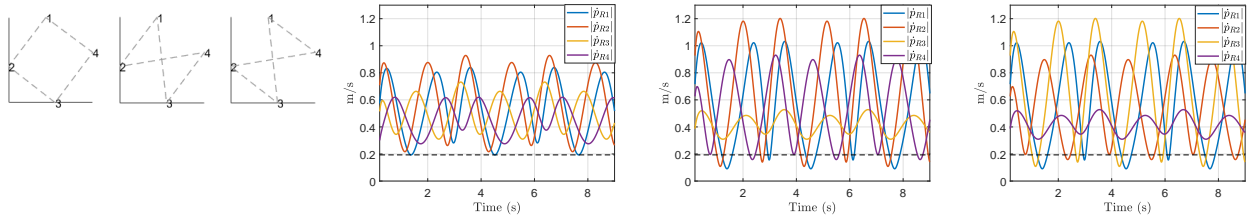


Figure 3. Simulation for the 3 Hamiltonian cycles of a 4-carrier system. The cycles are in the first plot on the left; the carriers' velocities for each of the 3 cycles are reported, in the same order, in the other plots. The minimum of the carriers' velocities in the first cycle is indicated by a dashed line in the three plots. As expected, it is greater than the minimum carrier's velocity when the other two cycles are selected.

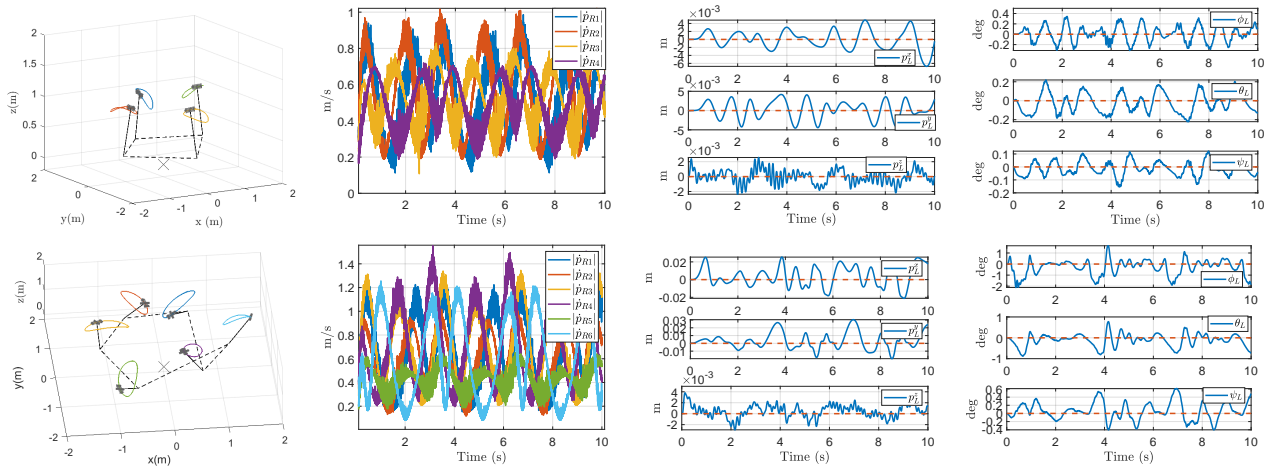


Figure 4. Four carriers (top row) 6 carriers (bottom row) manipulating a load. In the first column, a snapshot of an animation, where the carriers follow the colored planned paths, the cross indicates the load CoM, and dotted lines indicate the edges of the Hamiltonian cycle (connecting the cable anchoring point to the carrier on the corresponding graph vertex). In the second column, $|\dot{p}_{Ri}(t)| > 0$. In the third and fourth columns, the position and attitude of the load are reported.

Role of the Hamiltonian cycle on the load's pose error

This section focuses on the objective of leaving the pose of the suspended load unperturbed. The proposed algorithm provides nominal carriers' trajectories that do not perturb the load's equilibrium pose, in a similar way in which internal joint motions of a redundant robotic manipulator leave the end-effector still. However, there may be non-idealities such as noise, tracking errors, etc. that produce a motion of the load. Figures 4 report the results of 4 and 6 non-stop carriers keeping the load at its constant pose, where the roll, pitch, and yaw angles describing the load's attitude are respectively indicated as ϕ_L , θ_L , and ψ_L . The Hamiltonian cycles chosen to generate the internal forces are highlighted by the dotted lines, representing the graph's edges where the cable attachment points are the vertices. Note that the norm of each carrier velocity is always greater than zero during the task execution. In these and the following simulations,

the attachment points of the cables on the load are randomly generated in 3D around the position of its CoM and at different altitudes as follows:

$${}^B \mathbf{b}_i = [[\mathbf{Rz}(2\pi i/n + \zeta_i)[1.2, 0]^T]^T, \hat{z}_i]^T, \quad (30)$$

where $\mathbf{Rz}()$ is the elementary rotation around \mathbf{e}_3 , ζ_i is a random angle in $[0, 0.2]$ rad, and \hat{z}_i a random number in $[0, 1]$ m, and $n = 5$.

The phases of the periodic functions used to assign $\lambda_i(t)$ have been chosen as in Remark 5 to be able to test any Hamiltonian cycle.

We observe that noise and the carriers' tracking errors, resulting from the absence of a feedforward term, led to an acceptable error in the load's pose.

Moreover, we may expect that the load's pose error sensitivity to the non-idealities is different for different choices of the Hamiltonian cycle.

To assess this, we tested three different systems, all with $n = 5$ carriers. For each system, 12 simulations have been

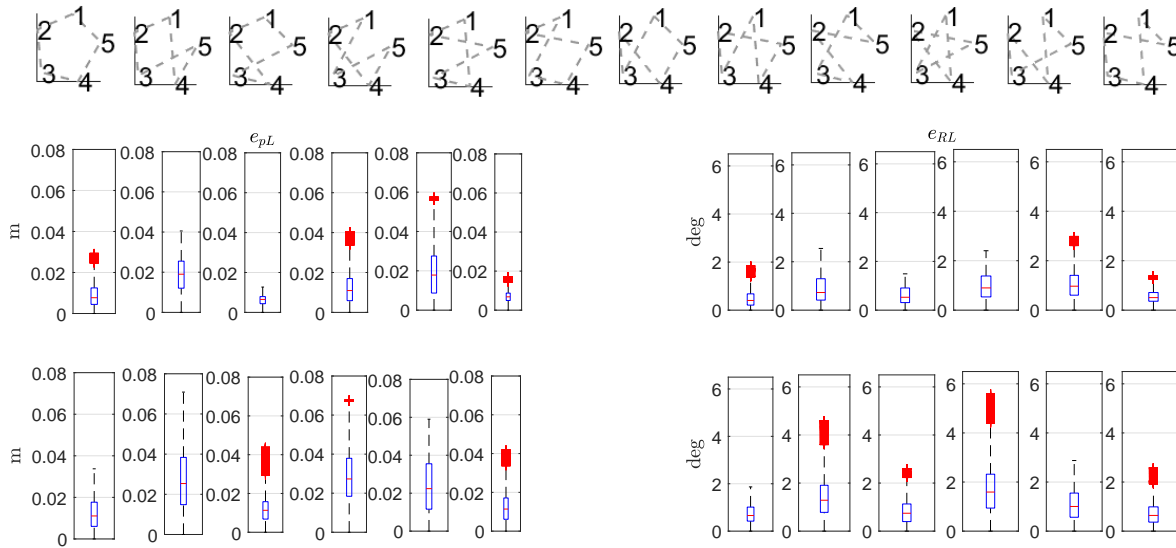


Figure 5. Results of 5-carrier system. Each column corresponds to one of the 12 Hamiltonian cycles, displayed in the first row, where the cable anchoring points of the load are displayed. The second row shows the values of e_{pL} and the third of e_{RL} .

run, one per each of the $(5 - 1)!/2 = 12$ Hamiltonian cycles. For the sake of space, being the outcomes of the three tests comparable, in Fig. 5 the results for one of the systems are reported, where we display the box plots of the position error computed as $e_{pL} = \|\mathbf{p}_L - \bar{\mathbf{p}}_L\|$ and of the attitude error $e_{RL} = |\psi_L| + |\theta_L| + |\phi_L|$ (desired yaw, pitch, and roll angle are equal to zero). These results suggest that the selection of the Hamiltonian cycle has an effect on the performance of the proposed method. However, for all systems, we observe that despite the choice of the Hamiltonian cycle, the load pose error is kept low, with peaks for the position error below 0.08 m and the attitude errors below 6 deg.

Conclusions and Future Work

This work demonstrated the compatibility of non-stop carrier flights with keeping constant the pose of cable-suspended loads for any $n \geq 3$ non-stop flying carriers. We proposed and formally derived a novel method to generate coordinated trajectories allowing the non-stop carriers to hold the load in a static equilibrium. We reported numerical results in support of the method.

Relevant future work concerns the design of an optimal planning algorithm that generates smooth non-stop trajectories accounting for obstacle avoidance and constraints on the state and input of the system, including fixed-wind carrier dynamics. Moreover, while this work is focused on the planning problem, with the control loop closed on the carriers' state, in the future, such trajectories could be embedded in an online optimization-based control method that closes the loop on the load state. This should allow bringing the load pose error to zero even in the presence of system uncertainties and disturbances. A more

realistic simulator will be developed to start assessing the practical applicability of the manipulation method. From an analytical point of view, the identification of families of trajectories compatible with the considered problem, and the rigorous study of how the method's parameters affect such trajectories remains an open and interesting point. Eventually, experimental tests will be carried out on non-stop flying carriers after considering possible necessary mechatronic adaptations.

References

1. Ruggiero, F., V. Lippiello, and A. Ollero. Aerial manipulation: A literature review. Vol. 3, No. 3, 2018, pp. 1957–1964.
2. Ollero, A., M. Tognon, A. Suarez, D. Lee, and A. Franchi. Past, present, and future of aerial robotic manipulators. Vol. 38, No. 1, 2021, pp. 626–645.
3. Estevez, J., G. Garate, J. M. Lopez-Guede, and M. Larrea. Review of Aerial Transportation of Suspended-Cable Payloads with Quadrotors. *Drones*, Vol. 8, No. 2. doi:10.3390/drones8020035.
4. Sreenath, K., N. Michael, and V. Kumar. Trajectory generation and control of a quadrotor with a cable-suspended load—a differentially-flat hybrid system. In *2013*. 2013, pp. 4888–4895.
5. Pereira, P. O., M. Herzog, and D. V. Dimarogonas. Slung load transportation with a single aerial vehicle and disturbance removal. In *2016 24th*. 2016, pp. 671–676.
6. Bernard, M. and K. Kondak. Generic slung load transportation system using small size helicopters. In *2009*. 2009, pp. 3258–3264.
7. Bernard, M., K. Kondak, I. Maza, and A. Ollero. Autonomous transportation and deployment with aerial robots for search and rescue missions. Vol. 28, No. 6, 2011, pp. 914–931.

8. Michael, N., J. Fink, and V. Kumar. Cooperative manipulation and transportation with aerial robots. Vol. 30, 2011, pp. 73–86.
9. Fink, J., N. Michael, S. Kim, and V. Kumar. Planning and control for cooperative manipulation and transportation with aerial robots. In *14th*. Springer, 2011, pp. 643–659.
10. Li, G., R. Ge, and G. Loianno. Cooperative transportation of cable suspended payloads with mavs using monocular vision and inertial sensing. Vol. 6, No. 3, 2021, pp. 5316–5323.
11. Gassner, M., T. Cieslewski, and D. Scaramuzza. Dynamic collaboration without communication: Vision-based cable-suspended load transport with two quadrotors. In *2017*. 2017, pp. 5196–5202.
12. Wahba, K. and W. Hönig. Efficient Optimization-based Cable Force Allocation for Geometric Control of a Multirotor Team Transporting a Payload.
13. Goodman, J. and L. Colombo. Geometric control of two quadrotors carrying a rigid rod with elastic cables. Vol. 32, No. 5, 2022, p. 65.
14. Gabellieri, C., M. Tognon, D. Sanalidro, and A. Franchi. Equilibria, Stability, and Sensitivity for the Aerial Suspended Beam Robotic System Subject to Parameter Uncertainty.
15. Pereira, P. O., P. Roque, and D. V. Dimarogonas. Asymmetric collaborative bar stabilization tethered to two heterogeneous aerial vehicles. In *2018*. 2018, pp. 5247–5253.
16. Chen, T. and J. Shan. Cooperative Transportation of Cable-suspended Slender Payload Using Two Quadrotors. In *2019 IEEE Int. Conf. on Unmanned Systems*. 2019, pp. 432–437. doi: 10.1109/ICUS48101.2019.8995928.
17. Jiang, Q. and V. Kumar. The inverse kinematics of cooperative transport with multiple aerial robots. Vol. 29, No. 1, 2012, pp. 136–145.
18. Mohammadi, K., S. Sirouspour, and A. Grivani. Passivity-Based Control of Multiple Quadrotors Carrying a Cable-Suspended Payload. Vol. 27, No. 4, 2022, pp. 2390–2400. doi: 10.1109/TMECH.2021.3102522.
19. Masone, C., H. H. Bühlhoff, and P. Stegagno. Cooperative transportation of a payload using quadrotors: A reconfigurable cable-driven parallel robot. In *2016*. 2016, pp. 1623–1630. doi: 10.1109/IROS.2016.7759262.
20. Leutenegger, S., C. Hürzeler, A. K. Stowers, K. Alexis, M. W. Achtelik, D. Lentink, P. Y. Oh, and R. Siegwart. Flying robots. *Springer Handbook of Robotics*, 2016, pp. 623–670.
21. Gabellieri, C. and A. Franchi. On the Existence of Static Equilibria of a Cable-Suspended Load with Non-stopping Flying Carriers. In *2024*. Chania, Greece, 2024, pp. 638–644. doi:10.1109/ICUAS60882.2024.10556930.
22. Sanalidro, D., H. J. Savino, M. Tognon, J. Cortés, and A. Franchi. Full-pose manipulation control of a cable-suspended load with multiple UAVs under uncertainties. Vol. 5, No. 2, 2020, pp. 2185–2191.
23. Yoshikawa, T. Virtual truss model for characterization of internal forces for multiple finger grasps. Vol. 15, No. 5, 1999, pp. 941–947.
24. Tognon, M., C. Gabellieri, L. Pallottino, and A. Franchi. Aerial co-manipulation with cables: The role of internal force for equilibria, stability, and passivity. Vol. 3, No. 3, 2018, pp. 2577–2583.
25. Zelazo, D., A. Franchi, H. H. Bühlhoff, and P. R. Giordano. Decentralized Rigidity Maintenance Control with Range Measurements for Multi-Robot Systems. *The International Journal of Robotics Research*, Vol. 34, No. 1, 2015, pp. 105–128. doi:10.1177/0278364914546173.
26. Soifer, A. *The Mathematical Coloring Book*. Springer-Verlag, 2008.

Acknowledgements

This work was partially funded by the Horizon Europe research and innovation programs under agreement no. 101059875 (Flyflic) and agreement no. 101120732 (Autoassess).